Electronic Supplementary Information

# Monitoring dynamic photocatalytic activity of single CdS nanoparticles by lighting up $H_2$ nanobubbles with fluorescent dyes

Hua Su, Yimin Fang, Fangyuan Chen and Wei Wang*

State Key Laboratory of Analytical Chemistry for Life Science, School of Chemistry and Chemical Engineering, Nanjing University, Nanjing 210023, China

*Correspondence to: Wei Wang, E-mail: wei.wang@nju.edu.cn.

**Table of Contents**

## Materials and methods

### 1.1 Synthesis and characterizations of CdS nanoparticles (NPs)

CdS NPs were prepared via hydrothermal treatment of CdS precursors formed by a slow addition of 500 mL $Na_2S$ solution (0.14 M) into 400 mL $Cd(OAc)_2$ solution (0.14 M), according to previously reported procedures.[1-2] The obtained crude products were thoroughly washed with plenty of water and ethanol to remove residual precursors and dried in vacuum. The obtained yellow powders were then dispersed in pure water with the help of ultrasonic bath for about 5 min prior to use.

The transmission electron microscopy (TEM) and scanning electron microscopy (SEM) characterizations of CdS NPs were carried out by JEOL 2800 and JSM-7800F, respectively. SEM images of CdS NPs on the glass coverslip indicated that CdS NPs were evenly dispersed on the substrate (Figure S1a and b). X-ray diffraction (XRD) pattern of CdS NPs with five distinct peaks at 26.5°, 30.6°, 43.8°, 51.9° and 70.3° (Figure S1c), can be assigned to (111), (200), (220), (311) and (331) crystal plane of cubic phase of CdS (JCPDS89-0440), respectively.[3] The lattice fringes of 0.33 nm can be clearly observed in high-resolution TEM images (Figure S1d), corresponding to the crystal plane (111) of cubic phase CdS.[4-5] The EDS mapping further confirmed the existence of S and Cd element (Figure S1f and g).

### 1.2 TIRF microscopy setup

The microscopy setup was based on an Olympus IX83 inverted microscopy as shown in Figure S6, in which an Olympus TIRF (TIRF is short for total internal reflection fluorescence) illuminator was equipped with a 488-nm continuous-wave laser (OBIS LX-100 mW, Coherent). After collimated and focused in TIRF apparatus, the laser passed through a narrow bandpass filter (Semrock, FF02-482/18), reflected from a dichroic mirror (Semrock, Di02-R488) and illuminated the sample through an oil-immersed objective (100×-TIRF, Olympus). When the incident angle of the light beam at the coverslip-water interface is tuned higher than the critical angle $\theta_c$, total internal reflection phenomenon occurs. The penetration depth of generated evanescent field is ~200 nm from the interface and therefore a good contrast can be obtained, due to the effective reduction of the fluorescence (FL) signals from the bulk solution. Note that 561-nm OBIS laser and corresponding filter sets was adopted when imaging nanobubbles generated by the decomposition of $NaBH_4$ (Figure S11a), in order to avoid possible photocatalytic reactions on CdS nanoparticles induced by 488-nm laser.

In our experiment, the 488-nm laser was simultaneously utilized to trigger CdS NPs photocatalysis and excite the fluorogenic molecule Rhodamine 6G (R6G). An emission filter (Semrock, BLP01-532R) was used to filter the scattered light of 488-nm laser and pass the FL signals of R6G. An EMCCD camera (Andor897, 512×512 pixels, 16 $\mu$m per pixel) was used to collect the FL signals with a usual gain value of 200. Using an Olympus ZDC equipment (ZDC is short for $z$-drift compensation), the focus stability of objective lens can be kept more than 10 hours. For the drift of sample stage on the $x$–$y$ plane, an image processing algorithm was used to correct the drift based on FL marker (2-D Gaussian fitting of the

marker at each frame). For bubble size calculation, a two-fold magnification lens (Olympus) was also used to further broaden the spot.

### 1.3 CdS NPs photocatalysis experiments on TIRF microscopy

No. 1 type glass coverslip (ThermoFisher, Catalog No. 12-542-B, 130 – 170 $\mu$m-thick) was successively washed by acetone, ethanol and water in an ultrasonic bath and were then placed in a newly prepared piranha solution for more than 12 h to remove organic adsorbates. After washed carefully with water and blown dry by $N_2$, the glasses were incubated in 1% (w/w) Poly-diallyldimethylammonium chloride (PDDA) aqueous solution for 1 h. Washed with plenty of water and dried in $N_2$ again, the glasses were assembled with a PDMS chamber (FlexiPERM micro 12) for CdS NPs immobilization and photocatalysis experiment. In order to immobilize CdS NPs on the coverslip, 100 $\mu$L of CdS dispersions (5 $\mu$g mL$^{-1}$) were added to the chamber and dried in vacuum at 50 $^{o}$C overnight. The resultant CdS NPs were firmly immobilized onto the positively charged PDDA-modified substrate, even under vigorously washing with plenty of $H_2O$ or 1M $Na_2S$-$Na_2SO_3$ aqueous solution.

Prior to experiments, an equal volume of newly-prepared $Na_2S$ solution (2 M) and $Na_2SO_3$ solution (2 M) was mixed and passed through a 0.22 $\mu$m filter to remove the insolubles. The filtered solution was then added into equal volume of R6G solution (50 $\mu$M) and mixed vigorously followed by a centrifugation process (14800 rpm for twice) to remove the produced aggregates. In a typical experiment, 270 $\mu$L reaction medium (pre-saturated with $H_2$) was added into the reaction chamber and another clean coverslip was used to cover it. After a short period (10 – 30 minutes) of illumination by 488-nm laser, random and frequent growth-and-drop in the FL intensity can be observed from camera, indicating a state of oversaturation of $H_2$ concentration and the nanobubble formation. It should be noted that the operating power of 488-nm laser ranged from 5 to 60 mW was often optimized to balance the signal-to-noise ratio and photochemical stability of CdS NPs. Higher laser power leads to better image quality but is more likely to inactivate CdS nanoparticle due to photocorrosion.

### 1.4 Confocal laser scanning fluorescence (FL) imaging of $H_2$ bubble

Macro-sized $H_2$ bubbles with sub-millimeter diameter were produced by spontaneous $NaBH_4$ decomposition in the presence of 1M $Na_2SO_3$ aqueous solution containing 2.5 $\mu$M R6G on the CdS and PDDA-modified coverslip. No $Na_2S$ was added because the presence of this strongly reducing agent was found to significantly inhibit the decomposition rate of $NaBH_4$. Resulted sub-millimeter bubbles were subsequently characterized with confocal laser scanning microscopy (Leica TCS SP5, 10×objective, excitation wavelength 488 nm). Ring-shaped patterns were typically observed, suggesting the accumulation of R6G at the nanobubble surface (Figure S3a).

## Supporting figures

**Figure S1. SEM, XRD and TEM characterizations of CdS NPs**

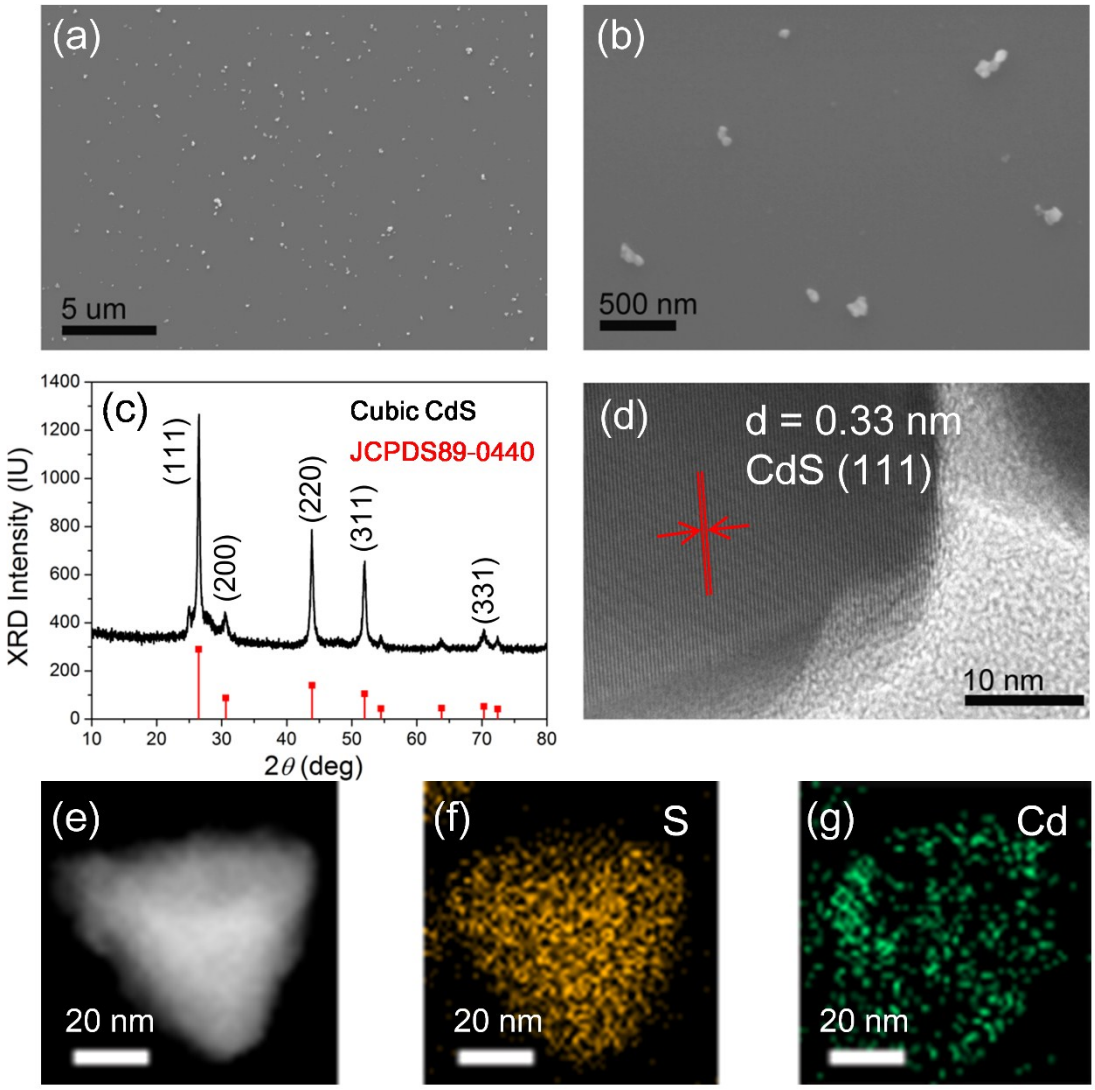


**Figure S1.** SEM, XRD and TEM characterizations of CdS NPs. SEM images of CdS NPs on the glass coverslip are shown at low (a) and high (b) magnification, respectively, indicating the CdS NPs are evenly and sparsely attached on the substrate. XRD pattern (c) indicates a cubic phase of CdS (JCPDS89-0440). (d) High-resolution TEM images of CdS NPs on carbon film-supported copper grid. (e-g) HAADF-STEM images of a CdS NP and the corresponding EDS mapping for S and Cd elements.

**Figure S2. Measurement of photocatalytic $H_2$ generation activity of CdS NPs using traditional ensemble method**

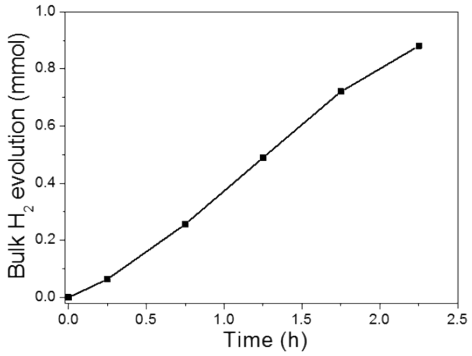


**Figure S2.** Hydrogen production activity of CdS NPs at ensemble level using a conventional photocatalysis system (Perfectlight, Labsolar Ⅲ-AG) equipped with a Xe lamp and gas chromatography. The experiment was performed in the presence of 30 mL volume (5 mg CdS NPs dispersed in a mixed solution of 0.5 M $Na_2S$ and 0.5 M $Na_2SO_3$) under blue light irradiation ($\lambda$<500 nm, 14 mW $mm^{-2}$). The bulk measurement indicated the as-obtained CdS NPs with a $H_2$ evolution rate of approximately 78.4 mmol $h^{-1}$ $g^{-1}$. Accordingly, the $H_2$ generation rate of single CdS NPs can be estimated to be 1.1X$10^5$ $H_2$ molecules/s (assuming an average CdS NPs diameter of 150 nm).

**Figure S3. FL imaging of a macro-sized $H_2$ bubble labeled by Rhodamine 6G (R6G)**

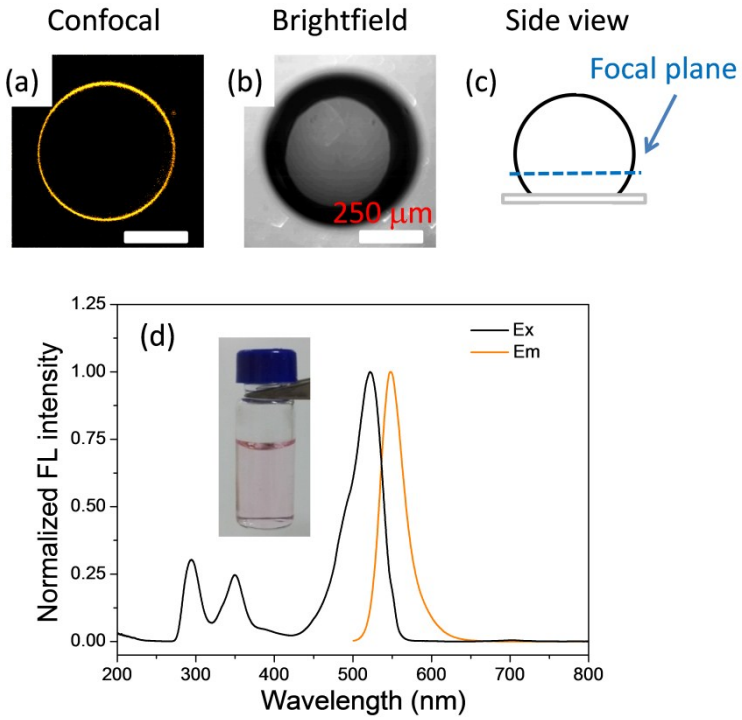


**Figure S3.** Confocal laser scanning fluorescence (a) and bright-field (b) images of a macro-sized bubble. Scale bar: 250 $\mu$m. (c) Focal plane is located at the lower portion of nanobubble as indicated in the side-view. The sub-millimeter bubble was produced by $NaBH_4$ decomposition (see Experimental section 1.4 for details). (d) Excitation and emission spectrum of R6G in 500 mM $Na_2S$-$Na_2SO_3$ aqueous solution. Excitation spectrum was recorded at 550 nm emission wavelength and emission spectrum is excited at 488 nm. Inset in (d) shows the optical photograph of as-prepared R6G-$Na_2S$-$Na_2SO_3$ solution.

**Figure S4. R6G control experiment for verifying the function of R6G dyes**

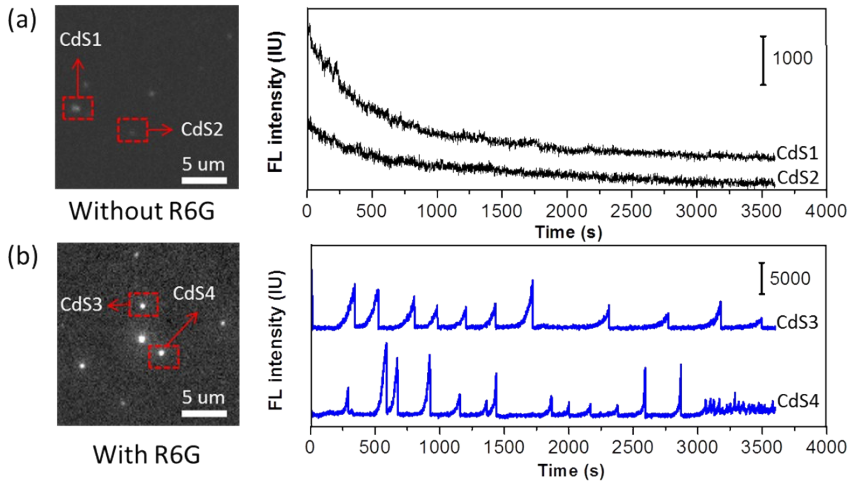


**Figure S4.** FL images and typical FL intensity trajectories of CdS in the absence and presence of R6G dyes under the same experimental conditions. (a) Intrinsic fluorescence intensity of CdS nanoparticles was much weaker than that of R6G-labeled nanobubbles and decreased gradually upon light exposure. In contrast, in the presence of R6G, monotonic increase followed by a rapid drop to its original value in the FL intensity appeared on single CdS NPs (b).

**Figure S5. Correlated SEM characterization and FL imaging evidenced that the nanobubbles were generated on the CdS NPs**

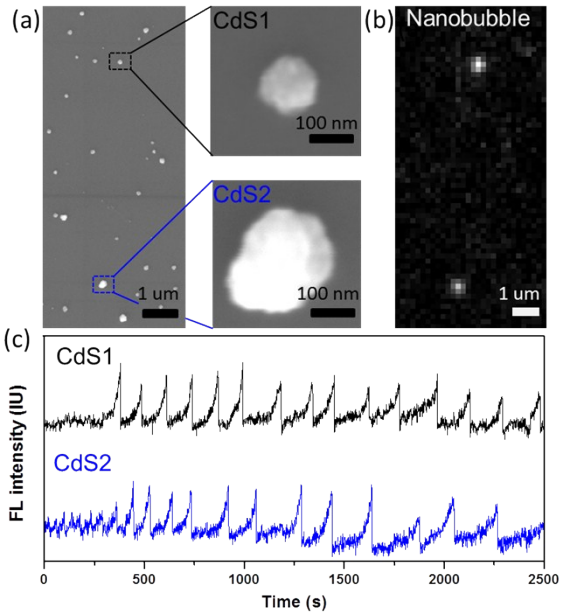


**Figure S5.** Correlated SEM characterization of CdS NPs and FL imaging of nanobubble generated on the same CdS NPs. (a) SEM images of CdS NPs show that CdS NPs with the size of about 100-200 nm are sparsely immobilized on the cover glass. (b) shows typical FL image of nanobubbles generated on the two CdS NPs, with the position of which are identical to that of SEM image in (a) to accurately determine the size of CdS NPs. The FL intensity trajectories of two nanobubble generated on the very same CdS NPs in (a) are recorded in (c).

**Figure S6. Detailed optical configuration of TIRF microscopy**

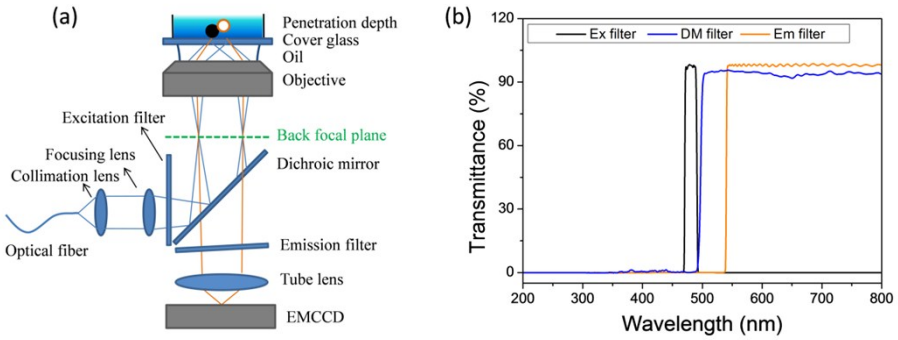


**Figure S6.** (a) Detailed optical configuration of the TIRF microscopy we adopted in the present work. (b) Transmittance spectrum of excitation filter (Ex filter, Semrock, FF02-482/18), dichroic mirror (DM filter, Semrock, Di02-R488) and emission filter (Em filter, Semrock, BLP01-532R).

**Figure S7. TIRF imaging vs wide-field epi-FL imaging**

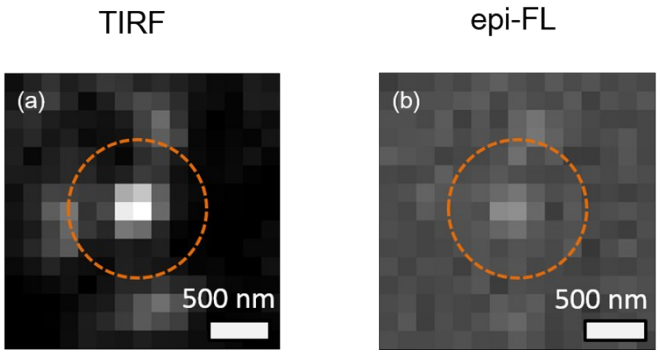


**Figure S7.** Comparison of TIRF (a) and epi-FL (b) imaging modes for nanobubbles generated by the same CdS NP. It is clear that better signal-to-noise ratio (image contrast) is obtained under TIRF mode because evanescent wave in TIRF significantly reduces the excitation volume and thus decreases the background FL emission. Scale bar: 500 nm.

**Figure S8. Nanobubble collapse kinetics recorded with a temporal resolution of 23 ms**

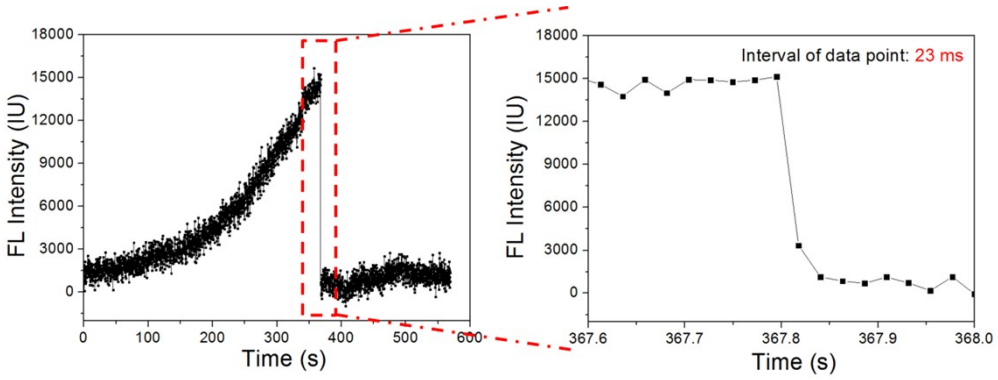


**Figure S8.** Dynamic process of the sudden collapse of nanobubble is recorded at a rate of 44 frames per second (corresponding to a temporal resolution of 23 milliseconds). Results show that it takes less than 23 milliseconds to dissolve the nanobubble.

**Figure S9. Statistical analysis of growth rates of 398 nanobubbles on 31 CdS NPs**

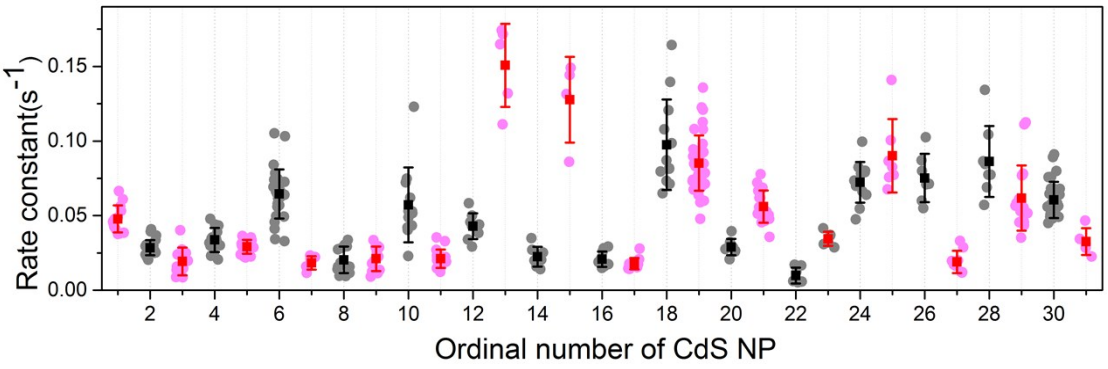


**Figure S9.** Statistical analysis of growth rate of 398 nanobubbles on 31 CdS NPs in a recording period of 1 h. The bubble growth rate was obtained by exponentially fitting the mean FL intensity of each bubble. The mean bubble growth rate on each CdS NPs was also shown with the standard deviation. While each nanobubble event exhibits varied growth rate, overall (averaged) growth rates are different from nanoparticle to nanoparticle.

**Figure S10. FWHM analysis of quantum dots (standard sample) and FL-labeled nanobubbles**

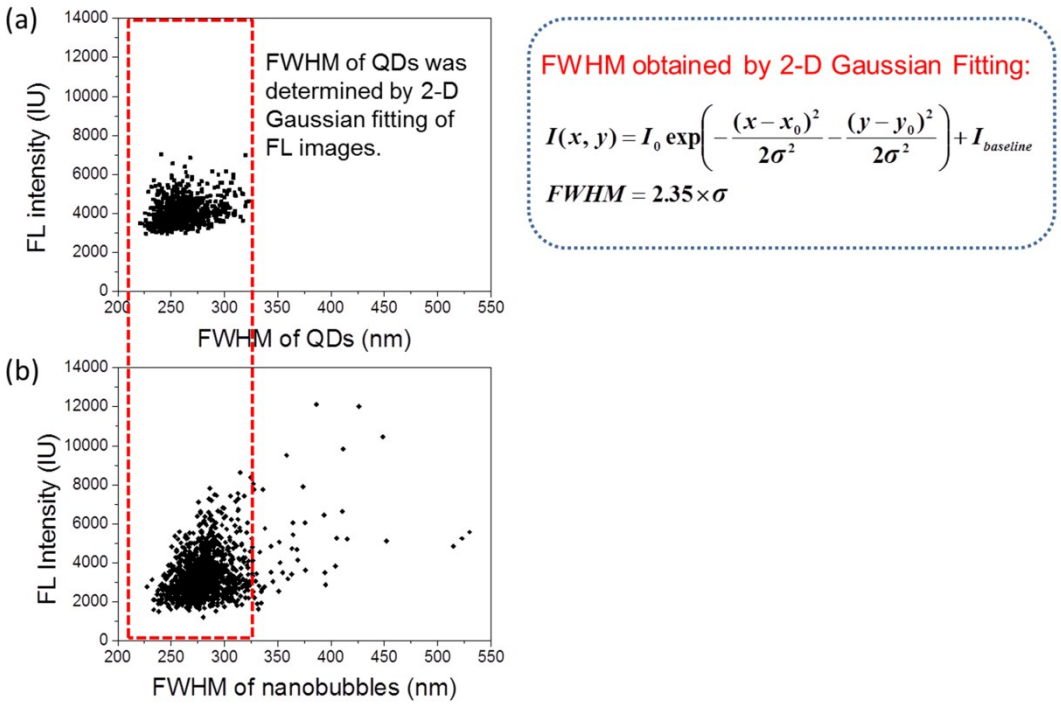


**Figure S10.** Correlation between FWHM value and FL intensity of quantum dots (a) and nanobubbles (b). 705 and 732 objects are analyzed for quantum dots and nanobubbles, respectively. Surface-immobilized quantum dots served as standard sample to demonstrate the size of point-spreading function (PSF) of TIRF microscope. Small percentage (~5%) of nanobubbles exhibits FWHM values larger than the diffraction limit, which can be used to quantify the actual size of nanobubbles. The commercial CdSe@ZnS core/shell quantum dots (Wuhan Jiayuan Quantum Dots Co., Ltd, Wuhan, China) immobilized on PDDA-modified coverslip were utilized as standard sample.

**Figure S11. FL trajectories of CdS NPs under the condition of $NaBH_4$ decomposition**

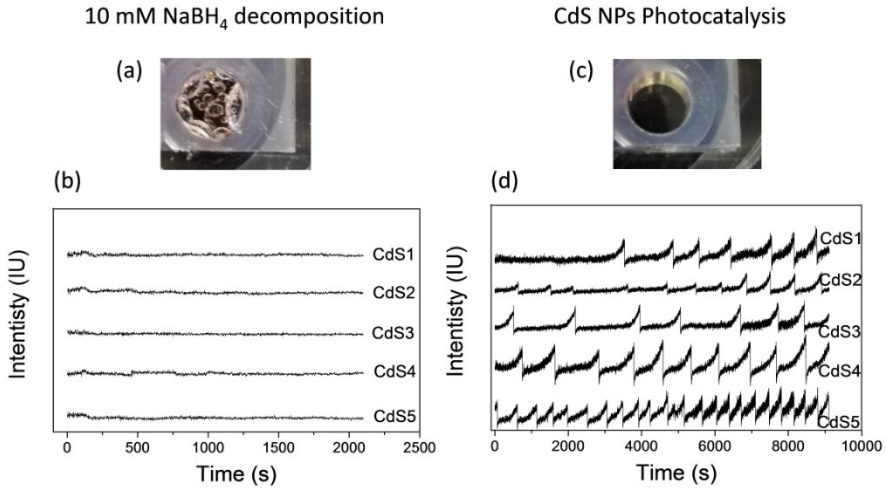


**Figure S11.** FL trajectory curves of five representative CdS nanoparticles under the condition of (a) decomposition of 10 mM $NaBH_4$ and (b) photocatalysis. In the $NaBH_4$ scenario, no nanobubble is detected at the surface of CdS nanoparticles even if the solution has been clearly saturated with $H_2$. After removal of $NaBH_4$ solution and addition of reaction medium for photocatalysis, the same CdS NPs exhibited dynamic nanobubbles formation and collapse behaviors. These results demonstrate that the nucleation and growth of solution-phase $H_2$ molecules at the surface of CdS nanoparticles are prohibited, even though a saturation of $H_2$ has been achieved in the bulk solution.

**Figure S12. Dependence of nanobubble growth rates on the operating power of laser**

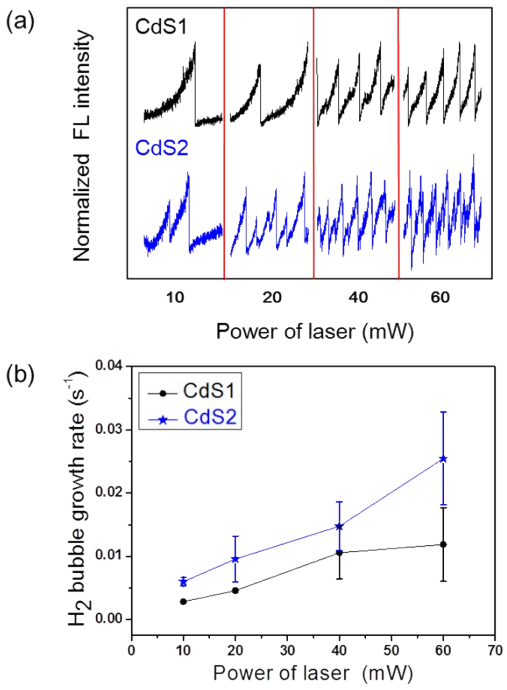


**Figure S12.** (a) Representative FL trajectories of two CdS nanoparticles under different laser power. (b) Averaged nanobubble growth rate is found to increase with the increasing laser power. Higher illumination density accelerates the photochemical reaction rates, leading to higher nanobubble growth rate.

**Figure S13. Effect of $H_2$ pre-saturation on the induction time of nanobubble generation**

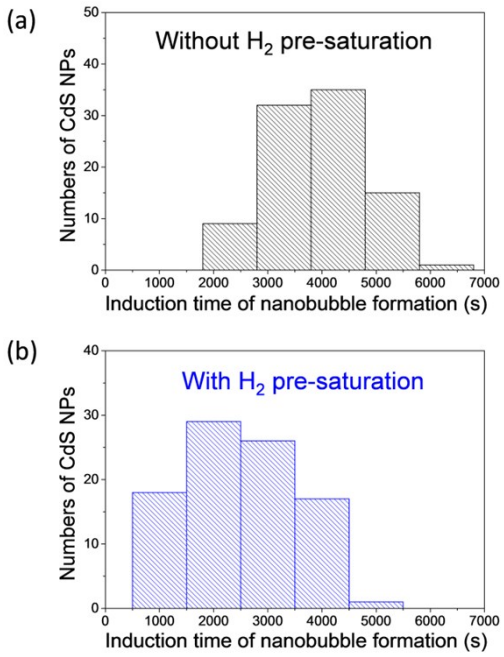


**Figure S13.** Induction time is often required to observe the nanobubble events. During this period of time, photo-generated $H_2$ molecules saturated the local medium, which is a prerequisite for nanobubble production. (a) When reaction medium is not pre-saturated with $H_2$, the averaged induction time is ~4000 seconds. This number is reduced to ~2000 seconds when the reaction medium is pre-saturated with $H_2$ molecules. The induction time was defined as the period from the beginning of light irradiation to the appearance of the first nanobubble collapse. 92 CdS NPs were analyzed for each case above.

## Supporting movie

**Movie S1:** A movie showing the time elapsed FL images and the corresponding FL trajectroies of nanobubbles generated on the two adjacent CdS NPs during photocatalysis in 1000 seconds.

## References


1. H. Yan, J. Yang, G. Ma, G. Wu, X. Zong, Z. Lei, J. Shi and C. Li, *J. Catal.*, 2009, **266**, 165-168.
2. Y. Fang, Z. Li, Y. Jiang, X. Wang, H.-Y. Chen, N. Tao and W. Wang, *Proc. Natl. Acad. Sci. U. S. A.*, 2017, **114**, 10566-10571.
3. L. Wu, J. C. Yu and X. Fu, *J. Mol. Catal. A: Chem.*, 2006, **244**, 25-32.
4. W. Shenton, T. Douglas, M. Young, G. Stubbs and S. Mann, *Adv. Mater.*, 1999, **11**, 253-256.
5. J. He, Z. Yan, J. Wang, J. Xie, L. Jiang, Y. Shi, F. Yuan, F. Yu and Y. Sun, *Chem. Commun.*, 2013, **49**, 6761-6763.